ISSN 1674-1056
http://cpb.iphy.ac.cn
http://iopscience.iop.org/cpb
中国物理 B
Chinese Physics
中国物理
Chinese Physics B

Interaction between human telomeric G-quadruplexes characterized by single molecule magnetic tweezers

Yi-Zhou Wang(王一舟), Xi-Miao Hou(侯锡苗), Hai-Peng Ju(车海鹏), Xue Xiao(肖雪), Xu-Guang Xi(奚绪光), Shuo-Xing Dou(窦硕星), Peng-Ye Wang(王鹏业), Wei Li(李伟)
Citation: Chin. Phys. B . 2018, 27(6): 068701. **doi:** 10.1088/1674-1056/27/6/068701

Journal homepage: http://cpb.iphy.ac.cn; http://iopscience.iop.org/cpb

What follows is a list of articles you may be interested in

Application of microdosimetry on biological physics for ionizing radiation

Dandan Chen(陈丹丹), Liang Sun(孙亮)
Chin. Phys. B . 2018, 27(2): 028701. **doi:** 10.1088/1674-1056/27/2/028701

Improved data analysis method of single-molecule experiments based on probability optimization

Weili Zhai(翟伟利), Guohua Yuan(袁国华), Chao Liu(刘超), Hu Chen(陈虎)
Chin. Phys. B . 2018, 27(1): 018703. **doi:** 10.1088/1674-1056/27/1/018703

Modulation and control of DNA charge inversion

Yan-Wei Wang(王艳伟), Guang-Can Yang(杨光参)
Chin. Phys. B . 2017, 26(12): 128706. **doi:** 10.1088/1674-1056/26/12/128706

Bloom's syndrome protein unfolding G-quadruplexes in two pathways

Zhen-Ye Zhao(赵振业), Chun-Hua Xu(徐春华), Jing Shi(史婧), Jing-Hua Li(李菁华), Jian-Bing Ma(马建兵), Qi Jia(贾棋), Dong-Fei Ma(马东飞), Ming Li(李明), Ying Lu(陆颖)
Chin. Phys. B . 2017, 26(8): 088701. **doi:** 10.1088/1674-1056/26/8/088701

Mechano-chemical selections of two competitive unfolding pathways of a single DNA i-motif

Xu Yue, Chen Hu, Qu Yu-Jie, Artem K. Efremov, Li Ming, Ouyang Zhong-Can, Liu Dong-Sheng, Yan Jie
Chin. Phys. B . 2014, 23(6): 068702. **doi:** 10.1088/1674-1056/23/6/068702

Interaction between human telomeric G-quadruplexes characterized by single molecule magnetic tweezers*

Yi-Zhou Wang(王一舟)[1,3,†], Xi-Miao Hou(侯锡苗)[2,†], Hai-Peng Ju(车海鹏)[1], Xue Xiao(肖雪)[1,3], Xu-Guang Xi(奚绪光)[2], Shuo-Xing Dou(窦硕星)[1,3], Peng-Ye Wang(王鹏业)[1,3,‡], and Wei Li(李伟)[1,§]

[1] *Key Laboratory of Soft Matter Physics, Beijing National Laboratory for Condensed Matter Physics, Institute of Physics, Chinese Academy of Sciences, Beijing* 100190, *China*

[2] *School of Life Sciences, Northwest A & F University, Yangling* 712100, *China*

[3] *School of Physical Sciences, University of Chinese Academy of Sciences, Beijing* 100049, *China*

(Received 25 December 2017; revised manuscript received 21 March 2018; published online 10 May 2018)

Human telomeric G-quadruplex plays a crucial role in regulating the genome stability. Despite extensive studies on structures and kinetics of monomeric G-quadruplex, the interaction between G-quadruplexes is still in debate. In this work, we employ magnetic tweezers to investigate the folding and unfolding kinetics of two contiguous G-quadruplexes in 100-mM K^+ buffer. The interaction between G-quadruplexes and the consequent effect on the kinetics of G-quadruplex are revealed. The linker sequence between G-quadruplexes is further found to play an important role in the interaction between two G-quadruplexes. Our results provide a high-resolution insight into kinetics of multimeric G-quadruplexes and genome stability.

Keywords: biophysics, G-quadruplexes, single-molecule studies, DNA structures

PACS: 87.80.Nj, 87.14.gk, 87.15.H– **DOI:** 10.1088/1674-1056/27/6/068701

1. Introduction

In human cells, telomeres at the termini of chromosomes are composed of tandemly repeated sequence 5'-TTAGGG and terminate with a single-strand 3'-overhang of approximately 200 nucleotides.[1] These repetitive sequences form multiple G-quadruplexes,[2,3] which are stacked with two or more G-quartets containing four coplanar guanines through Hoogsteen hydrogen bonds.[4,5] The G-quadruplex array can protect the chromosomes from damaging and end-fusing,[6] playing crucial functions in regulating the chromosome stability, gene transcription, recombination, and replication.[7–10]

Extensive studies have been carried out on the structures and kinetics of monomeric G-quadruplex including DNA G-quadruplex[11–13] and RNA G-quadruplex.[14] The highly polymorphic structures of G-quadruplex are revealed, including the parallel, anti-parallel, hybrid-1 and hybrid-2 structure.[15–17] Recently, single molecular methods including optic tweezers, magnetic tweezers and FRET have been employed for investigating the folding kinetics of monomeric G-quadruplex.[11–13,18,19] All these studies revealed the monomeric G-quadruplex folding and unfolding mechanism at the molecular level and gave deeper insights into the telomere maintenance and design of ligands for anti-cancer purposes.

However, whether the interaction between G-quadruplexes exists, the crucial question for understanding the higher order of multimeric G-quadruplexes, is still in debate. Thermodynamics assays indicated an unfavorable coupling free energy in the multimeric assembly of G-quadruplexes,[20,21] while molecular simulation studies[22] and photoreaction assays[23] suggested the existence of stable interaction between two hybrid-type G-quadruplexes. Recently, the mechanic unfolding assays by optic tweezers on the full length human telomeric overhang show most of G-quadruplexes are independent, while a minor population of higher-order interactions between G-quadruplexes are observed.[24] These controversial results indicate that the interaction between G-quadruplexes is far from being understood.

Single molecule methods provide a powerful tool to investigate the kinetics of G-quadruplex, which helps to elucidate whether the interaction between G-quadruplexes exists and how the interaction affects the kinetics of G-quadruplexes. In this work, we construct the simplest multimeric system with two G-quadruplexes *in vitro* and investigate the folding and unfolding kinetics of the two contiguous G-quadruplexes in 100-mM K^+ buffer by using magnetic tweezers. In our experiment, two dinstinct unfolding modes are observed, implying

*Project supported by the National Natural Science Foundation of China (Grant Nos. 11474346 and 11774407), the Key Research Program of Frontier Sciences, Chinese Academy of Sciences (Grant No. QYZDB-SSW-SLH045), and the National Key Research and Development Program, China (Grant No. 2016YFA0301500).

†These authors contributed equally to this work.

‡Corresponding author. E-mail: pywang@iphy.ac.cn

§Corresponding author. E-mail: weili007@iphy.ac.cn

© 2018 Chinese Physical Society and IOP Publishing Ltd

the existence of the interaction between two G-quadruplexes. Interestingly, the interaction destablizes one G-quadruplex unit and stablizes the other. Besides, we also demonstrate that the TTA linker plays a crucial role in the interaction between G-quadruplexes. Our findings shed light on the stability and interaction mechanism of G-quadruplexes at human telomeres, which should be helpful for understanding the regulation of gemone stability.

2. Materials and methods

2.1. Preparation of DNA construct

The DNA construct contains three parts: a 699-bp double strand DNA handle with biotin modification, a single strand telomeric DNA sequence 5'-GGG(TTAGGG)$_7$(wtTel45) and a 2271-bp double strand DNA handle with digoxigenin modification. The contour length of the DNA construct is ~ 1 μm. Two handles were prepared by PCR amplification of PBR322 with primers. The PCR products were purified by a QIAquick PCR Purification Kit (QIAGEN, Germany), and then digested by XbaI and KpnI (Ipswich, MA) respectively. The digested products were further purified using the QIAquick PCR Purification Kit, and the concentrations of handle products were determined with a UV spectrophotometer. To ligate single strand DNAs with handles, the ssDNA that can form one or two telomeric G-quadruplexes (blue) was annealed with flank 1 and flank 2 in 1:1:1 ratio by slowly cooling down from 95 °C to 25 °C, then ligated with two dsDNA handles in 1:1:1 ratio by T4 ligase at 16 °C overnight. Finally, Agarose gels were performed to check the final product, and the DNA constructs were stored at −20 °C.

2.2. Magnetic tweezers stretching experiment

Our single molecule manipulation experiments were performed by magnetic tweezers. As shown in Fig. 1(a), the two ends of the DNA construct are tethered via digoxigenin and anti-digoxigenin ligation to a glass coverslip and via biotin-streptavidin ligation to a 1-μm diameter Dynabeads (Invitrogen Norway). Two small NdFeB magnets on the DNA constructs are controlled to pull on the Dynabeads and thus stretch the DNA molecule. The real time position of the bead is monitored by a JAI Giga-Ethernet CCD camera at 60 Hz through an inverted microscope objective (Olympus 100 × 1.2, oil immersion). The extension (end to end distance) of the DNA construct is determined at nanometer resolution by analyzing the diffraction pattern of Dynabeads.[25] The 1-μm diameter polystyrene reference beads are stuck on the coverslip using nitrocellulose and tracked simultaneously to eliminate the shift of the device. To ensure that only one DNA construct was tethered to a bead, we rotated magnet pairs for ~ 50 turns at ~ 5 pN and checked whether the bead is rotation-constrained, namely, more than one DNA being tethered to the bead. Our magnetic tweezers were controlled by a home-built LabVIEW program. In the force ramp experiment, magnet pairs were moved at nonlinear step size to keep a constant loading rate. The step size can be calculated according to the force-magnet position relationship fitted with exponential function.[26,27] (see Appendix A "Force calibration")

2.3. Surface treatment and flow cell

To bound the reference beads, the inner surface of coverslips was coated with $\sim 0.2\%$ w/v nitrocellulose (Sigma-Aldrich) and 0.03% w/v polystyrene beads (ACMEmicrospheres) in alcohol and then heated at 150 °C for 5 min,[28] allowing the nitrocellulose solvent to evaporate and the polystyrene beads to melt onto the surface as reference beads. Afterwards, 10-mg/ml anti-digoxigenin was used to modify the surface overnight at 37 °C and then dealt with passivation buffer (10-mg/ml BSA, 1-mM EDTA, 10-mM pH 7.4 phosphate buffers, 10 mg/ml Pluronic F127 surfactant (Sigma-Aldrich), 3-mM NaN_3)at room temperature for 4 h to avoid non-specific ligation between magnetic beads and the surface. In our experiments, the DNA constructs were diluted to 40 pM and blended with 10× diluted Dynabeads MyOne in 1:1 volume ratio for 30 min. The DNA-bead mixture was injected into the flow cell and incubated for 30 min, then rinsing away the unconnected beads with TE buffer.

3. Results and discussion

3.1. Dimeric G-quadruplexes less stable than monomeric G-quadruplex

As shown in Fig. 1(a), the wildtype human telomeric G-quadruplex sequence (wtTel45) 5'-GGG(TTAGGG)$_7$ with a lower 699-bp dsDNA handle and an upper 2271-bp dsDNA handle is tethered specifically between an antidigoxigenin coated coverslip and a streptavidin-coated paramagnetic bead (MyOne Invitrogen). Force exerted on the paramagnetic bead is tuned by adjusting the magnets vertically and the extension is traced at a nanometer resolution based on the diffraction image of the bead.[25] To demonstrate that our sample can form two contiguous G-quadruplexes, force jump experiments were performed. Figure 1(b) shows the force-jump experiments between 0.1 pN and 7 pN and two extension steps around 9 nm reveal two G-quadruplex ruptures at the high tension. According to other single molecule experiments on double strand DNA (dsDNA), conformation change cannot occur when the force is less than 60 pN.[29–34] Repeated measurements and similar results reveal that two stable G-quadruplexes are formed in the wtTel45 sequence, which is consistent with the results previously reported by AFM and NMR.[35,36]

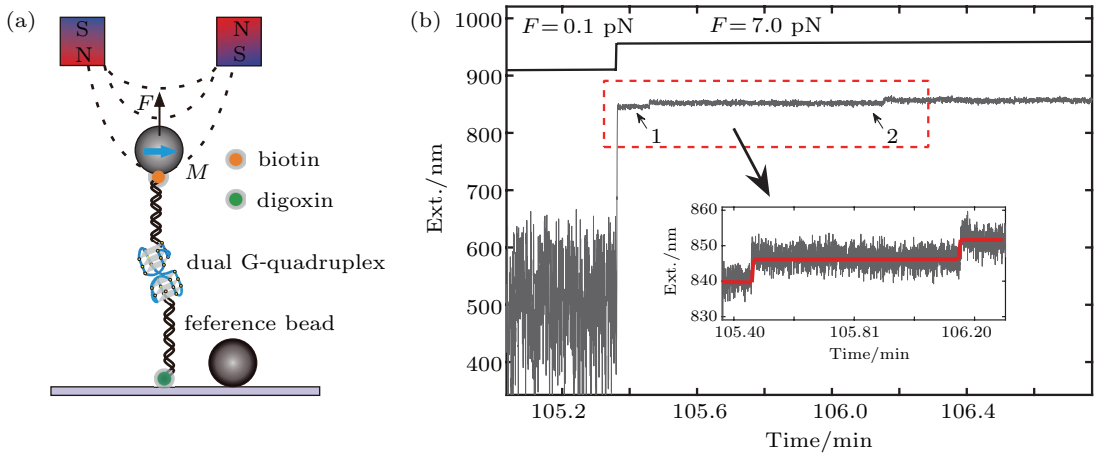


Fig. 1. (color online) (a) Schematic setup of magnetic tweezers (not to scale). The 45 nt wtTel45 sequence is tethered between a coverslip and a superparamagnetic bead with two 699 bp and 2271 bp dsDNA handles. (b) Typical trajectory with two distinct ruptures indicate two stable G-quadruplexes formed in wtTel45 sequence.

To further quantify the two G-quadruplex ruptures formed in wtTel45 sequence, we perform the force-ramp experiments from 0.7 pN to 8.3 pN at the loading rate $r = 0.16$ pN/s. As shown in Fig. 2(a), two sequential extension jumps in each trajectory correspond to the unfolding of two G-quadruplexes, which is consistent with the result of previous force-jump experiment (Fig. 1(b)). For clarity, the trajectories are shifted in extension. The first rupture event, which happens with co-existence of the other G-quadruplex, is a key target for the investigation of the interaction between the G-quadruplexes. We repeat the force-ramp measurement and derive the unfolding force distribution p for the first G-quadruplex rupture as shown in the upper panel of Fig. 2(b).

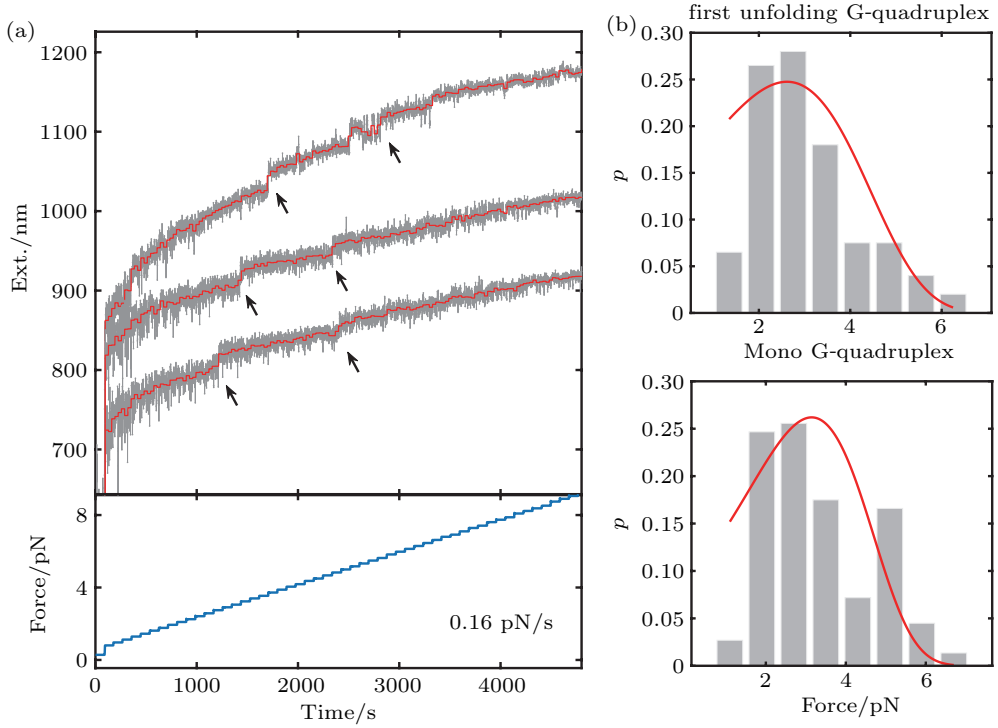


Fig. 2. (color online) Force ramp experiments of dimeric G-quadruplexes and mono G-quadruplex. (a) Typical force responses of dual G-quadruplexes in a stretching cycle (upper panel) with a loading rate of.16 pN/s (lower panel). (b) Unfolding force distribution of the first G-quadruplex in the dimeric G-quadruplexes fitted with Evans model (upper panel, $N = 200$) and monomeric G-quadruplex (lower panel, $N = 198$).

To compare the tension response of G-quadruplex in the presence and in the absence of another G-quadruplex, the same force-ramp measurements are performed on the monomeric G-quadruplex formed in wtTel21 sequence 5'-GGG(TTAGGG)$_3$ (see Appendix A in Fig. S3). The corresponding unfolding force distribution p of monomeric G-quadruplex is shown in the lower panel in Fig. 2(b). Compared with the monomeric G-quadruplex, the first ruptured G-quadruplex in the wtTel45 sequence prefers to unfold at lower forces. The experiment shows that the mechanical stability of G-quadruplex is atten-

uated by the existence of another G-quadruplex, which suggests the existence of interaction between G-quadruplexes. Our results agree well with the reported results that dimeric G-quadruplexes melt before monomeric G-quadruplex in previous CD thermal analysis.[22,37]

In our force-ramp measurement, the force distribution in the force spectroscopy measurements of single molecules can be described by Evans' model[38] as follows:

$$p_{\text{unfold}} = \frac{k_{\text{u}}^0}{r}\exp\left(\frac{F\Delta x_{\text{u}}}{k_{\text{B}}T}\right) \times \exp\left\{\frac{k_{\text{u}}^0 k_{\text{B}}T}{\Delta x_{\text{u}} r}\left[1-\exp\left(\frac{F\Delta x_{\text{u}}}{k_{\text{B}}T}\right)\right]\right\}, \quad (1)$$

where r is the loading rate, F is the external tension, k_{B} is the Boltzmann constant, and T is the absolute temperature. The k_{u}^0 corresponding to the unfolding rate at $F = 0$ pN and Δx_{u} corresponding to the distance between the folded state and the reaction energy barrier in the reaction coordinate, are treated as the fitting parameters. The best fitting parameters of the first unfolding G-quadruplex are $k_{\text{u}}^0 = (2.6 \pm 1.1) \times 10^2$ s^{-1}, $\Delta x_{\text{u}} = 2.1 \pm 0.7$ nm (mean $\pm$ SD), and the best fitting parameters of monomeric G-quadruplex are $k_{\text{u1}}^0 = (1.7 \pm 0.9) \times 10^2$ s^{-1}, $\Delta x_{\text{u1}} = 2.5 \pm 0.8$ nm. The first G-quadruplex in the wtTel45 sequence presents higher unfolding rate k_{u}^0 (at $F = 0$ pN) and lower unfolding force (Fig. 2(b)) than the monomeric G-quadruplex, which also indicates that the G-quadruplex in the wtTel45 sequence is less stable in the presence of another G-quadruplex due to the interaction between the G-quadruplexes. It should be noted that the reaction distance Δx determined in the force ramp experiment is a little larger than results in Refs. [39] and [40]. A possible explanation is that Bell's model is no longer valid at low transition forces at such a slow loading rate, because it ignores the entropic elastic contribution in transition kinetics that is often significant at low forces.[41]

3.2. Distinct unfolding kinetics suggesting the interaction between two contiguous G-quadruplexes

To reveal the interaction between the two G-quadruplexes and to understand the consequence effect on the G-quadruplex, the force clamp measurement is performed by tracing the folding and unfolding kinetics of the dimeric G-quadruplexes at different forces. As shown in Fig. 3(a), the length of the samples are traced from 1.7 pN to 8 pN. At each tension, the measurement is sustained for fifteen min, which provides an adequate time to reveal the folding and unfolding kinetics of the G-quadruplex at a given tension. Two different unfolding processes are distinguished (the green and yellow regions for the first and second unfolding process respectively in Fig. 3(a)), which correspond to the sequential ruptures of the two formed G-quadruplexes in the wtTel45 sequence. The folding and unfolding transition of G-quadruplex are controlled by the external tension that tilts the equilibrium of G-quadruplex from folded state to unfolded state.

The reversible hopping behavior provides a framework for unraveling the different kinetics of two G-quadruplexes formed in the wtTel45 sequence. At a constant tension near the unfolding tension, G-quadruplex hops between folded and unfolded state. The unfolding rate k_{u} from folded to unfolded state can be described as an Arrhenius-like expression[31,32]

$$k_{\text{u}} = k_{\text{u}}^0 \exp\left(\frac{\Delta x_{\text{u}} F}{k_{\text{B}}T}\right), \quad (2)$$

where F is the external tension, k_{B} is the Boltzmann constant, and T is the absolute temperature. A similar relationship for the folding rate k_{f} can be calculated accordingly. The unfolded rate k_{u} increases and the folded rate k_{f} decreases with the increase of tension as shown in Fig. 3(b). At the equilibrium force F_{eq}, G-quadruplex hops between the folded and unfolded states with the same rate $k_{\text{u}} = k_{\text{f}}$ and the average dwelling time τ_0 of the folded state is equal to that of the unfolded state. In Fig. 3(b), the equilibrium force F_{eq} can be read from the point where the folded rate k_{f} (red line) equals the unfolded rate k_{u} (blue line). Near F_{eq}, the folding and unfolding kinetics of the first and second G-quadruplexes are shown in Fig. 3(c), corresponding to the region marked with a black rectangle in Fig. 3(a). The values of average dwelling time τ_0 are 20.5 s and 4.0 s for the first and second G-quadruplex, respectively (Fig. 3(c)). The average dwelling time of the first G-quadruplex, much larger than that of the second G-quadruplex at F_{eq}, indicates the slower folding and unfolding kinetics at the equilibrium tension in the presence of another G-quadruplex. We perform the same measurement for the monomeric G-quadruplex, and the average dwelling time $\tau_0 = 2.7$ s at F_{eq} is revealed, which is similar to that of the second G-quadruplex in the wtTel45 sequence (see Appendix A, Fig. S4 online). Unlike the monomeric G-quadruplex and the second unfolding G-quadruplex, the first unfolding G-quadruplex shows slower folding and unfolding kinetics, suggesting the existence of the interaction between G-quadruplexes.

By analyzing the different kinetics of the two G-quadruplexes formed in the wtTel45 sequence, we derive the free energy ΔG_0, an important quantity describing the stability of G-quadruplex. The relationship between the equilibrium rate constant $k_{\text{eq}} = k_{\text{u}}/k_{\text{f}}$ and external tension F can be described as

$$k_{\text{eq}} = k_{\text{eq}}^0 \exp\left(\frac{\Delta G(F)}{k_{\text{B}}T}\right), \quad (3)$$

where k_{eq}^0 is the equilibrium rate constant at $F = 0$ pN, $\Delta G(F) = F\Delta x + \Delta\Phi(F)$ is the free energy cost for unfolding

the G-quadruplex, and

$$\Delta\Phi(F) = -\int_0^{F_{\rm eq}} \left[x_{\rm ssDNA}(F') - x_{\rm G4}(F')\right] {\rm d}F'$$

accounts for the force-dependent entropic free energy change.[18] To calculate $\Delta\Phi(F)$ the ssDNA force-extension curve $x_{\rm ssDNA}(F)$ can be described by a phenomenological model[42] as follows:

$$x_{\rm ssDNA}(F) = h\left(\frac{a_1 \ln(F/f_1)}{1 + a_3 \exp(-F/f_2)} - a_2 - \frac{F}{f_3}\right), \quad (4)$$

where the empirical parameters $h = 0.34$ nm, $a_1 = 0.21$, $a_2 = 0.34$, $f_1 = 0.0037$ pN, $f_2 = 2.9$ pN, and $f_3 = 8000$ pN. The salt dependent parameter $a_3 = 2.1 \ln([K^+]/0.0025)/\ln(0.15/0.0025)$, where $[K^+]$ is the salt concentration. The project length along the force direction of folded G-quadruplex is given by

$$x_{\rm G4}(F) = l_0 \coth\left(\frac{F l_0}{k_{\rm B}T}\right) - \frac{k_{\rm B}T}{F},$$

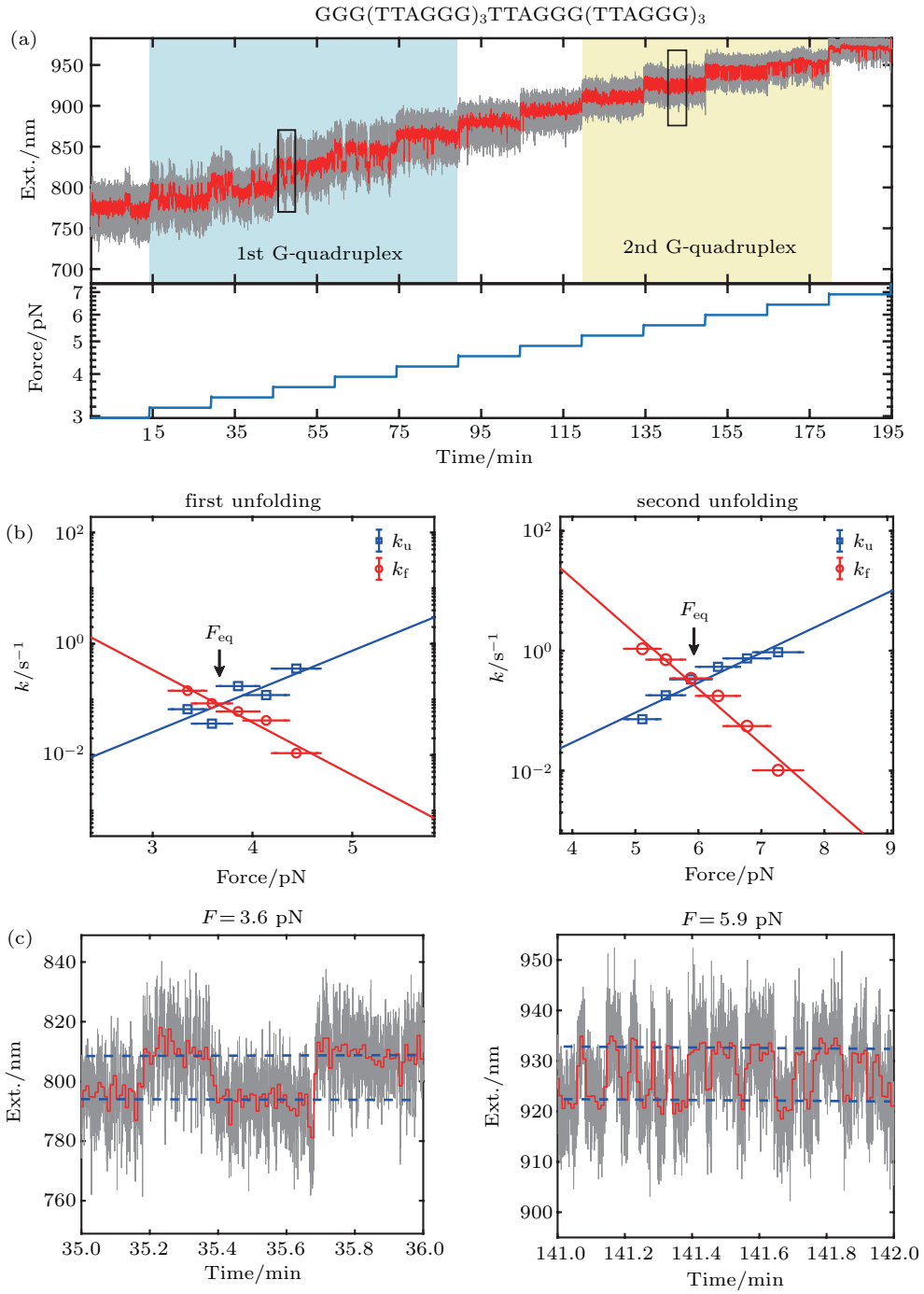


Fig. 3. (color online) Folding and unfolding kinetics of two G-quadruplexes in wtTel45 sequence. (a) Trajectory (upper panel) under different constant forces (lower panel) showing two ruptures of G-quadruplex. (b) Relationships between reaction rate k_u, k_f, and tension F. The equilibrium tension F_{eq} can be read from the point where $k_u = k_f$. The error bars reflect a $\sim 10\%$ error in force determination. (c) Different folding and unfolding kinetics of two G-quadruplex near F_{eq}. For the first G-quadruplex, $\tau_0 = 20.5$ s (left panel) and for the second G-quadruplex, $\tau_0 = 4.0$ s (right panel).

where $l \sim 1.7$ nm.[18] At F_{eq} such that $k_{eq} = k_u/k_f = 1$, we can derive free energy difference ΔG_0 by calculating the value of $\Delta\Phi(F_{eq})$. From the equation above, the values of free energy ΔG_0 for the first and second G-quadruplex in the wtTel45 sequence are obtained to be $2.9k_BT$ and $5.0k_BT$ respectively. For the monomeric G-quadruplex, the free energy ΔG_0 is $3.6k_BT$. The lower free energy of the first G-quadruplex reveals that the interaction between G-quadruplexes weakens the stability of G-quadruplex.

3.3. Effect of linker DNA on interaction between two G-quadruplexes

In the wtTel45 sequence, the two G-quadruplexes are connected via a TTA linker, which is suggested to play an important role in the interaction between two contiguous G-quadruplexes.[22] We construct the mutant Tel45 sequence by replacing the TTA linker with an AAA linker and perform the measurements as shown in Fig. 4. In a representative trajectory, two sequential reversible unfolding processes are observed, corresponding to the two G-quadruplexes formed in

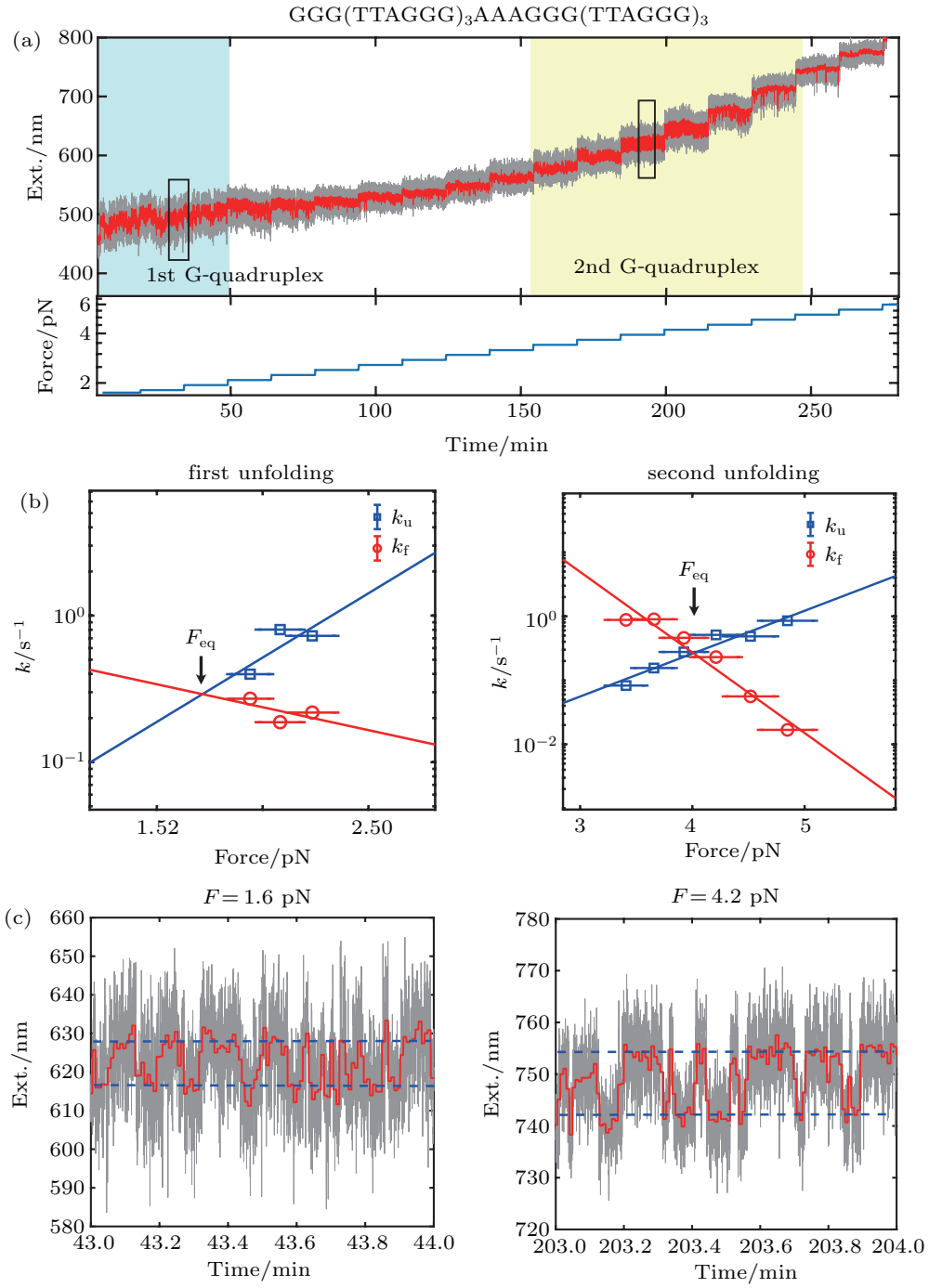


Fig. 4. (color online) Folding and unfolding kinetics of two G-quadruplexes in mutant Tel45 sequence. (a) Trajectories (upper panel) under different constant tensions (lower panel) show two ruptures of G-quadruplex. (b) Relationships between rate constant k_u, k_f, and tension F. (c) Near F_{eq}, similar folding and unfolding kinetics of G-quadruplex. For the first G-quadruplex, $\tau_0 = 4.2$ s (left panel), and for the second G-quadruplex, $\tau_0 = 3.6$ s (right panel).

the mutant Tel45 sequence (Fig. 4(a)). By plotting the folding and unfolding rate constant versus force, we obtain the equilibrium forces 1.6 pN and 4.1 pN for the first and second unfolding G-quadruplex in the mutant Tel45 sequence respectively (Fig. 4(b)). Compared with G-quadruplexes formed in the wtTel45 sequence, the two G-quadruplexes in the mutant Tel45 sequence show a relatively small equilibrium force, implying two less stable G-quadruplexes in the mutant Tel45 sequence. Near F_{eq}, the two G-quadruplexes hop between folded and unfolded state with a similar rate. The values of average dwelling time τ for the first and second G-quadruplex are 4.2 s and 3.6 s respectively (Fig. 4(c)), which are similar to that of the monomeric G-quadruplex, indicating similar folding and unfolding kinetics of the G-quadruplex in the mutant Tel45 sequence to those of the monomeric G-quadruplex. Our results demonstrate that the TTA linker plays a crucial role in the interaction between G-quadruplexes, which is consistent with previous simulation.[22]

4. Conclusion and perspectives

In this work, we investigate the interaction between two G-quadruplexes formed in the wtTel45 sequence by magnetic tweezers. In the presence of another G-quadruplex, G-quadruplex is less stable and unfolded at lower tension. The different folding and unfolding kinetics of the two G-quadruplexes formed in the wtTel45 sequence due to the interaction between the G-quadruplexes are further revealed. All the work indicates that the interaction between G-quadruplexes exists and the interaction affects the kinetics of the G-quadruplex. We further reveal that the linker between G-quadruplexes is an important factor for the interaction in the force clamp experiments for the mutant Tel45 sample; however, the reason for the interaction is complicated. We perform the force clamp experiments on the $(TTAGGG)_4$ and $GGG(TTAGGG)_3TTA$ sequence, which form G-quadruplex with a TTA residue on 5' and 3' respectively (see Appendix A, Fig. S5 and Fig. S6 online). Both the two G-quadruplexes with TTA residue have similar unfolding kinetics to the monomeric G-quadruplex ($\tau_0 = 2.7$ s), suggesting that the interaction is involved in two contiguous G-quadruplexes besides the TTA linker. It has been demonstrated that a long single strand G-rich DNA can form a higher order structure containing consecutive G-quadruplex. Our findings reveal the mechanism of G-quadruplex interaction, which should be helpful in the in-depth understanding of the telomeric G-quadruplex stability and regulation in vivo.

Appendix A: Supplementary information

A1. DNA oligonucleotides

Oligonucleotides were purchased from Sangon (Shanghai, China) in desalted, lyophilized form. They were dissolved in TE buffer (10-mM Tris-HCl, 1-mM EDTA, and 100-mM K^+, pH = 8.0). Concentrations of nucleotides were measured by UV spectrophotometer from their absorbance at 260 nm. The single strand telomeric DNA sequence are as follows:

Dimeric Gquadruplexes oligo:

5'-phosphate-CTAGCGGTGTGAAATACCGACACAGGGTTAGGGTTAGGGTTAGGGTTAGGGTTAGGGTTAGGTTAGG GACAGCCAGCAAGACGTAGCCAGCT

Monomeric G-quadruplex oligo:

5'-phosphate-CTAGCGGTGTGAAATACCGACACAGGGTTAGGGTTAGGGTTAGGGACAGCCAGCAAGACGTAGCCA GCT

Dimeric G-quadruplexes mutant oligo:

5'-phosphate-CTAGCGGTGTGAAATACCGACACAGGGTTAGGGTTAGGGTTAGGGAAAGGGTTAGGGTTAGGGTTA GGGACAGCCAGCAAGACGTAGCCAGCT

Flank 1 and Flank 2:

5'-TGTGTCGGTATTTCACACCG

5'-GGCTACGTCTTGCTGGCTGT

Primers for preparing handles:

5'-biotin-CGGGAGGGCTTACCAT

5'-GCTCTAGAGCCATACCAAACGACGAG

5'-CGAGCTCCCTGACGAGCATCACAAA

5-digoxigenin-GCCATACCAAACGACGAG

A2. Force calibration

In traditional force calibration of magnet tweezers, the force exerted on DNA molecules is calibrated based on the thermal fluctuation of the beads by the formula:

$$F = \frac{k_B T \langle z \rangle}{\langle \delta x^2 \rangle},$$

where k_B is the Boltzmann constant, T is the absolute temperature, z is the extension of DNA construct along the direction of force, and δx^2 is the variance of the fluctuation along a direction perpendicular to the force.[43] Because of the limit of our sampling rate, it is difficult to measure force accurately beyond 10 pN for a $\sim$ 1-μm DNA tether.[44] We introduced an approximation that the same vertical force is exerted on all the beads in the record scope of CCD at the same time, thus the force only depends on the position of magnet pairs. 48502 bp λ-DNA molecules were used to calibrate the force at different magnet position (Z_{mag}) because longer DNA tether could improve the accuracy of force at the same sampling rate. The data of 10 individual λ-DNA is shown in Fig. S1. Each force point was calculated by a horizontal bead trajectory of 4096 frames. A single exponential function was used empirically to fit the force-z_{mag} relationship.[45] Considering the inconformity of bead magnetic moment and the error of z_{mag}, the relative error of force was estimated $\sim$ 10%.

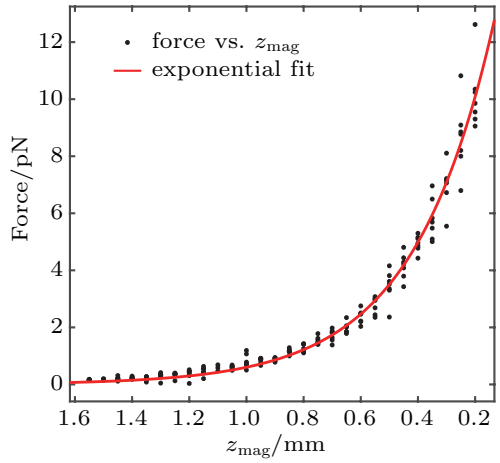


Fig. S1. (color online) Force-z_{mag} plot (black) obtained from 10 individual λ-DNA molecules and single exponential fitting curve (red).

A3. Smoothing of data

To identify the folding/unfolding events in recorded trajectories, the thermal motion along the force direction was firstly removed using the 5-level Harr wavelet transform tool in MATLAB, as shown in Fig. S2(a). The step size folding and unfolding transitions at constant force were detected using a chi-square step detect algorithm, which was optimized for detect transition step under constant force.[46]

A4. Dwell time analysis

Dwell time distribution of folding/unfolding state (Fig. S2(b)) were obtained by recording the lifetime of every fitted state, and thus fitted with a single exponential function. The force-dependent folding rate $k_f(F)$ and unfolding rate $k_u(F)$ are determined by fitting parameters of the single exponential function as:

$$p(F) = \exp\left[-1/k(F)\right].$$

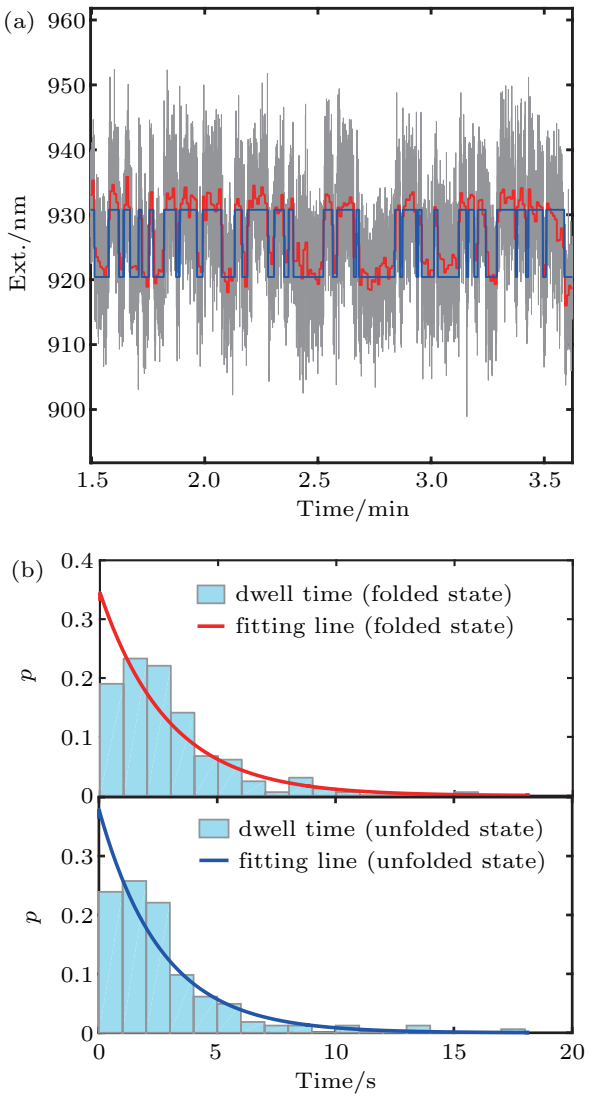


Fig. S2. (color online) Smoothing of data and dwell time analysis. (a) Typical recorded trajectory at constant force (gray). Red line shows the wavelet de-noised data and blue line shows the fitting result of step-detect algorithm. (b) Dwell time distribution (cyan) and fitting line (red and blue) of the distribution in panel (a).

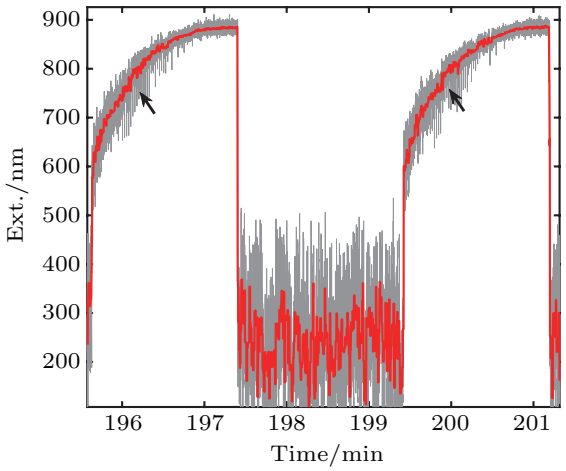


Fig. S3. (color online) Typical force ramp trajectories (gray) and smoothed data (red) of monomeric G4. The unfolding events are indicated with black arrows.

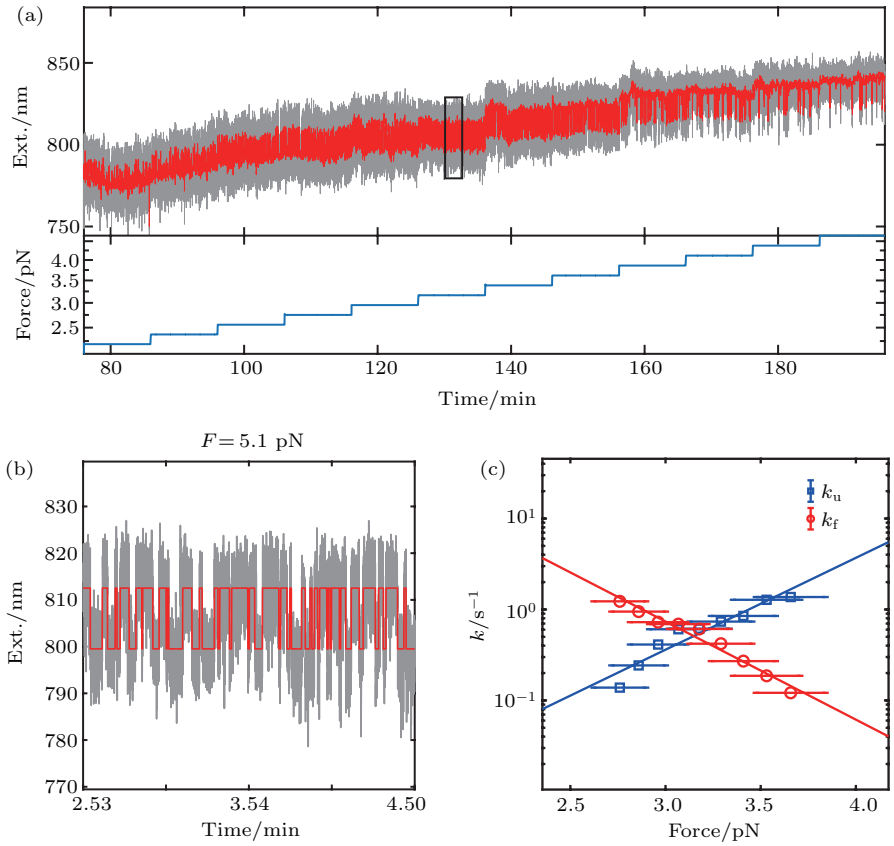


Fig. S4. (color online) Unfolding kinetics of monomeric G4. (a) Representative force responses (gray) and smooth data (red) of G4 formed by mt Tel21 at different constant force. (b) Zoom-in pictures of the rectangle in Figure S6A fitted with step detect algorithm. (c) Fitted folding rate k_f (red circle) and unfolding rate k_u (blue diamond) of G4. The x-axis error bars reflect a $\sim$ 10% error in force determination.

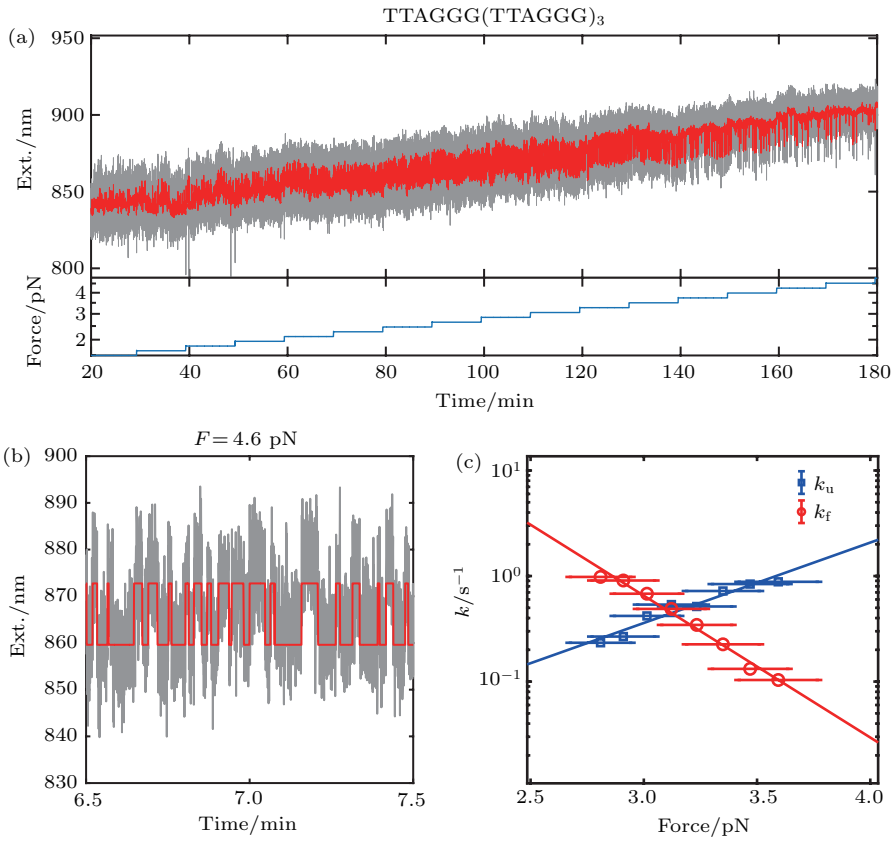


Fig. S5. (color online) Unfolding kinetics of TTA-G4. (a) Representative force responses (gray) and smooth data (red) of TTA-G4 formed by TTAGGG(GGGTTA)$_3$ at different force. (b) Folding and unfolding transitions of TTA-G4 at constant force. (c) Fitted folding rate k_f (red circle) and unfolding rate k_u (blue diamond) of TTA-G4. The x-axis error bars reflect a $\sim$ 10% error in force determination.

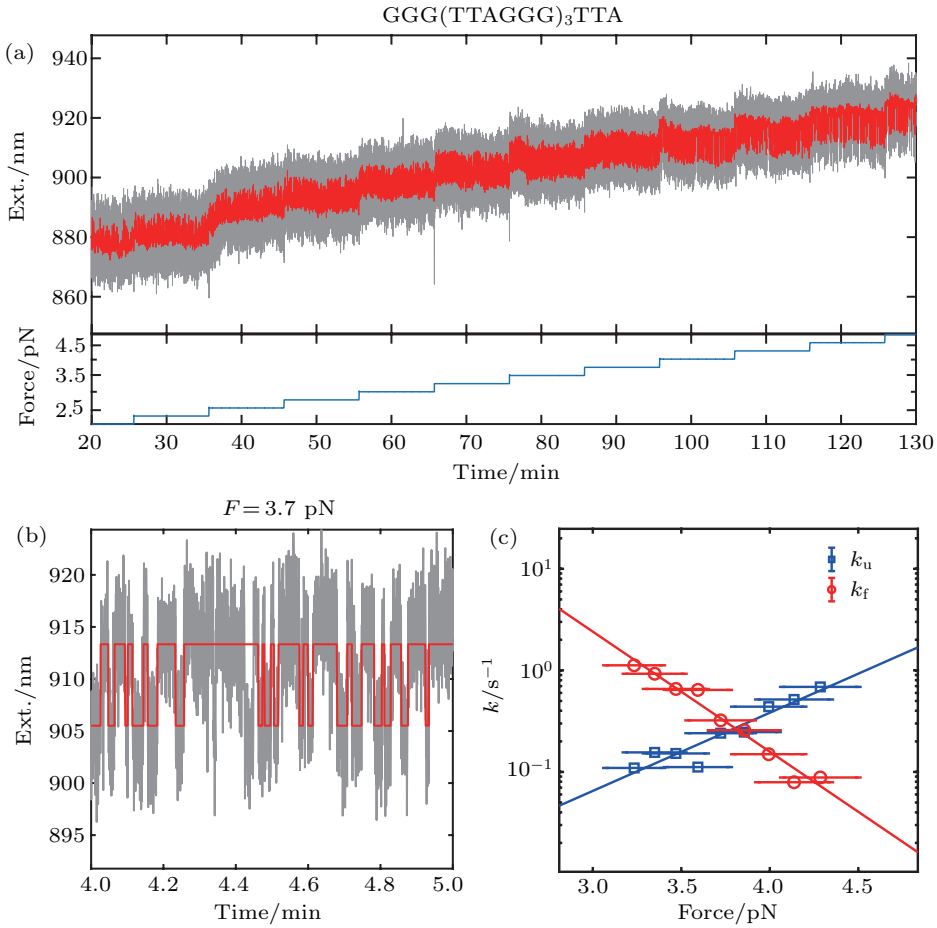


Fig. S6. (color online) Unfolding kinetics of G4-TTA. (a) Representative force responses (gray) and smooth data (red) of G4-TTA formed by GGG(TTAGGG)$_3$TTA at different force. (b) Folding and unfolding transitions of G4-TTA at constant force. (c) Fitted folding rate k_f (red circle) and unfolding rate k_u (blue diamond) of G4-TTA. The x-axis error bars reflect a $\sim 10\%$ error in force determination.

References

[1] Moyzis R K, Buckingham J M, Cram L S, Dani M, Deaven L L, Jones M D, Meyne J, Ratliff R L and Wu J R 1988 *Proc. Natl. Acad. Sci. USA* **85** 6622

[2] Biffi G, Tannahill D, McCafferty J and Balasubramanian S 2013 *Nat. Chem.* **5** 182

[3] Todd A K, Johnston M and Neidle S 2005 *Nucleic Acids Res.* **33** 2901

[4] Kaur P, Wu D, Lin J, Countryman P, Bradford K C, Erie D A, Riehn R, Opresko P L and Wang H 2016 *Sci. Rep.* **6** 20513

[5] Dai J, Carver M and Yang D 2008 *Biochimie* **90** 1172

[6] Maizels N 2006 *Nat. Struct. Mol. Biol.* **13** 1055

[7] Cahoon L A and Seifert H S 2009 *Science* **325** 764

[8] Rodriguez R, Miller K M, Forment J V, Bradshaw C R, Nikan M, Britton S, Oelschlaegel T, Xhemalce B, Balasubramanian S and Jackson S P 2012 *Nat. Chem. Biol.* **8** 301

[9] Siddiqui-Jain A, Grand C L, Bearss D J and Hurley L H 2002 *Proc. Natl. Acad. Sci. USA* **99** 11593

[10] Wang H, Nora G J, Ghodke H and Opresko P L 2011 *J. Biol. Chem.* **286** 7479

[11] Dhakal S, Cui Y, Koirala D, Ghimire C, Kushwaha S, Yu Z, Yangyuoru P M and Mao H 2013 *Nucleic Acids Res.* **41** 3915

[12] Gray R D, Buscaglia R and Chaires J B 2012 *J. Am. Chem. Soc.* **134** 16834

[13] Li W, Hou X-M M, Wang P-Y Y, Xi X G G and Li M 2013 *J. Am. Chem. Soc.* **135** 6423

[14] Laguerre A, Hukezalie K, Winckler P, Katranji F, Chanteloup G, Pirrotta M, Perrier-Cornet J M M, Wong J M and Monchaud D 2015 *J. Am. Chem. Soc.* **137** 8521

[15] Wang Y and Patel D J 1993 *Structure* **1** 263

[16] Parkinson G N, Lee M P and Neidle S 2002 *Nature* **417** 876

[17] Luu K N, Phan A T, Kuryavyi V, Lacroix L and Patel D J 2006 *J. Am. Chem. Soc.* **128** 9963

[18] You H, Zeng X, Xu Y, Lim C J, Efremov A K, Phan A T and Yan J 2014 *Nucleic Acids Res.* **42** 8789

[19] Ju H P, Wang Y Z, You J, Hou X M, Xi X G, Dou S X, Li W and Wang P Y 2016 *Acs. Omega.* **1** 244

[20] Petraccone L, Spink C, Trent J O, Garbett N C, Mekmaysy C S, Giancola C and Chaires J B 2011 *J. Am. Chem. Soc.* **133** 20951

[21] Yu H, Gu X, Nakano S-i, Miyoshi D and Sugimoto N 2012 *J. Am. Chem. Soc.* **134** 20060

[22] Petraccone L, Trent J O and Chaires J B 2008 *J. Am. Chem. Soc.* **130** 16530

[23] Li Y and Sugiyama H 2015 *Chem. Commun.* **51** 8861

[24] Abraham Punnoose J, Cui Y, Koirala D, Yangyuoru P M, Ghimire C, Shrestha P and Mao H 2014 *J. Am. Chem. Soc.* **136** 18062

[25] Lionnet T, Allemand J F F, Revyakin A, Strick T R, Saleh O A, Bensimon D and Croquette V 2012 *Cold. Spring. Harb. Protoc.* **2012** 34

[26] Chen H, Fu H, Zhu X, Cong P, Nakamura F and Yan J 2011 *Biophys. J.* **100** 517

[27] Zhao X, Zeng X, Lu C and Yan J 2017 *Nanotechnology* **28** 414002

[28] Cnossen J P, Dulin D and Dekker N H 2014 *Rev. Sci. Instrum.* **85** 103712

[29] Smith S B, Cui Y and Bustamante C 1996 *Science* **271** 795

[30] Cluzel P, Lebrun A, Heller C, Lavery R, Viovy J L, Chatenay D and Caron F 1996 *Science* **271** 792

[31] Fu H, Chen H, Marko J F and Yan J 2010 *Nucleic Acids Res.* **38** 5594

[32] Fu H, Chen H, Zhang X, Qu Y, Marko J F and Yan J 2011 *Nucleic Acids Res.* **39** 3473

[33] Zhang X, Chen H, Fu H, Doyle P S and Yan J 2012 *Proc. Natl. Acad. Sci. USA* **109** 8103
[34] Zhang X, Chen H, Le S, Rouzina I, Doyle P S and Yan J 2013 *Proc. Natl. Acad. Sci. USA* **110** 3865
[35] Xu Y, Ishizuka T, Kurabayashi K and Komiyama M 2009 *Angew. Chem. Int. Ed. Engl.* **48** 7833
[36] Hänsel R, Löhr F, Trantirek L and Dötsch V 2013 *J. Am. Chem. Soc.* **135** 2816
[37] Cousins A R, Ritson D, Sharma P, Stevens M F, Moses J E and Searle M S 2014 *Chem. Commun.* **50** 15202
[38] Evans E and Ritchie K 1997 *Biophys. J.* **72** 1541
[39] Dhakal S, Cui Y, Koirala D, Ghimire C, Kushwaha S, Yu Z, Yangyuoru P M and Mao H 2013 *Nucleic Acids Res.* **41** 3915
[40] You H, Zeng X, Xu Y, Lim C J, Efremov A K, Phan A T and Yan J 2014 *Nucleic Acids Res.* **42** 8789
[41] Yuan G, Le S, Yao M, Qian H, Zhou X, Yan J and Chen H 2017 *Angew. Chem. Int. Ed.* **56** 5490
[42] Cocco S, Yan J, Léger J-F F, Chatenay D and Marko J F 2004 *Phys. Rev. E* **70** 11910
[43] Strick T R, Allemand J F, Bensimon D, Bensimon A and Croquette V 1996 *Science* **271** 1835
[44] Chen and H *et al.* 2011 *Biophys. J.* **100** 517
[45] Lipfert J and Hao X and Dekker N H 2009 *Biophys. J.* **96** 5040
[46] Aggarwal T, Materassi D, Davison R, Hays T and Salapaka M 2012 *Cellular and Molecular Bioengineering* **5** 14